Green Energy Generation from the Industrial Waste Red Mud as Hydroelectric Cell

Jyoti Shah[†*], Sunidhi Badola[#^], Abha Shukla[#^], R K Kotnala[#^†]

[†]*New Science Creators Institute, NSCI, Delhi 110067 India*

[#]*CSIR-National Physical Laboratory, Dr. K. S. Krishnan Road, Delhi 110012 India*

[^]*Academy of Scientific and Innovative Research (AcSIR), Ghaziabad 201002, India*

Volume 2, Issue 1, February 2025
Received:10 February, 2025; Accepted: 26 February, 2025
DOI: https://doi.org/10.63015/2hec-2455.2.1

**Corresponding Author Email: shah.jyoti1@gmail.com*

Abstract: Red Mud is a highly alkaline and toxic waste product generated in large quantities during alumina refining. Huge quantities of red mud are improperly disposed off regularly, contaminating land, water, and air which pose alarming environmental challenges. Converting red mud to energy material for hydroelectric cell is a sustainable solution to save the environment. Red mud is translated to defective and porous structure by adding ZnS through solid state reaction process. Dislocation density in red mud crystallite found to be increased from 5.93 x10^4 to 13.03x10^4 by adding ZnS due to defects creation. SEM images clearly show increase in porous microstructure of the composite. Red mud based hydroelectric cell generated current 8 mA, and voltage 0.96 V that increased to 13 mA and 0.98 V by 10 wt% ZnS addition. Charge transfer resistance of red mud drastically decreased from 80.7 Ω to 4.4 Ω, thus decreased the activation loss and increased the current generated in red mud-ZnS composite. Transforming red mud into hydroelectric cell presents a sustainable waste-to-energy solution that could revolutionize energy security and environmental pollution.

Keywords: Red mud, Hydroelectric Cell, Green electricity, Defects, Waste utilization

1. Introduction: Continuous efforts to boost industrialisation and economic growth has put the environment on the back seat. The after effects of rapid urbanization that took place in the last few decades are now coming out at an alarming stage. The massive amount of waste generated by factories, refineries, industries, manufacturing units, energy production and other sectors is creating nuisance in the environment. Untreated waste disposal creates more harm by polluting the land, water and soil. One such industrial waste is Red Mud (RM), a residue produced during alumina refining by Bayer process. Solid waste red mud is highly alkaline complex mixture of many oxides that is generated in huge amounts in alumina refineries all over the world. For every tonne of refined alumina, around 1.5-2 tonnes of red mud is produced as a residue. Red mud, having pH 10-13, is highly toxic for all the life forms as well as the environment [1]. Red mud typically comprises 65-70% iron oxide, 40-50% aluminium oxide, and 15-25% titanium dioxide, with variations based on the bauxite source, along with many heavy metals like arsenic, lead, cadmium, mercury etc. Most of this hazardous waste, which also contains valuable materials, ends up in landfills or stored in massive man-made ponds. These create problems for the nearby living beings. Globally, there are more than 100 operational Bayer process plants, collectively generating a stockpile of over 3.5 billion tonnes of bauxite residue. The continuous and rapid accumulation of this by-product poses a significant threat to human health, plant life, and the environment. The toxic effects of such a waste product have compelled scientists and researchers to think about its utilization instead of disposal.

Over the time red mud have been utilized for the extraction of iron, titanium, and other rare earth elements through a variety of pyrometallurgical, direct reduction, and hydrometallurgical processes [2,3]. Red mud exhibits a pronounced capacity as an adsorbent for the effective sequestration of heavy metal, non-metal, and organic contaminants, as well as synthetic dyes from aqueous effluents [4,5]. Waste red mud is transformed into a high-performance supercapacitor electrode through mechanical milling, exhibiting excellent capacitance and stability, offering a sustainable solution for its disposal [6]. Inspite of the growing research for its utilization and recycling, industrial applications of red mud remain limited, with only 3-4% of total generation being utilized in sectors such as cement production, brick manufacturing, and iron ore supplementation.

An ingenious step in this direction is transforming the solid waste red mud into green energy generating device Hydroelectric Cell (HEC), that holds a high potential for its useful disposal [7]. The Hydroelectric cell works on the principle of water splitting by metal oxides/ferrites at room temperature [8]. Strategically created surface defects and nanopores enhance the water splitting efficiency of the material and aids in green electricity generation [9–14]. In this direction, present research work investigates the potential of red mud (RM), an industrial waste product, for water splitting without using any acid/alkali or light. Using a simple solid state reaction method,10 and 20 weight % ZnS was added to Red Mud, creating oxygen deficiencies and nano-porosity within its structure. The structure, morphology and power generation capacity of the Red mud based Hydroelectric cells have been studied by X-ray diffraction (XRD), Scanning Electron Microscopy (SEM), V-I polarization curves and Electrochemical Impedance Spectroscopy (EIS).

2. Materials & Method: The raw material, solid waste red mud was collected from a leading alumina refining company and washed with distilled water until a neutral pH 7 was obtained. Red mud and its composite with 10 and 20 wt % ZnS (Thomas Baker; 97% purity) were hand grinded with methanol solvent in a pestle-mortar for 30 minutes. The grinded powder was pressed in the shape of 1 inch square pellets and sintered at 800 °C for 2 hours. From the sintered pellets, Hydroelectric cells were fabricated by attaching zinc electrode on one face and conducting silver paste in comb pattern on the other face of the square pellet. Samples were labelled as RM (red mud), RMZ1 (10 wt % ZnS-Red Mud) and RMZ2 (20 wt % ZnS-Red Mud).

3. Characterization: The material properties have been studied using different characterization techniques. The X-ray diffraction spectra has been recorded on Bruker D8 Advance XRD with a 0.154 nm Cu-Kα radiation. The morphology of different samples has been studied using SEM images taken on Carl Zeiss Scanning Electron Microscope. The current-voltage characteristics of the fabricated Hydroelectric cells have been recorded using the Keithley 2430 1 kW power source meter. The ionic diffusion of different species and charge transfer phenomenon in the cell was investigated by Electrochemical Impedance spectroscopy using Wayne-Kerr 6500B impedance analyser, in the frequency range 20 Hz to 120 MHz.

4. Results and Discussion:

4.1. X-ray Diffraction (XRD): The crystalline phase and structural parameters of the samples have been determined through XRD measurements. The XRD spectra of RM, RMZ1 and RMZ2 are given in figure 1(a). Most XRD peaks of red mud match well with that of rhombohedral Fe_2O_3 confirmed by the ICDD card number 04-007-9266. A few peaks could also be indexed to ICDD card number 04-009-8445 indicating presence of $AlFeO_3$ phase [7]. On

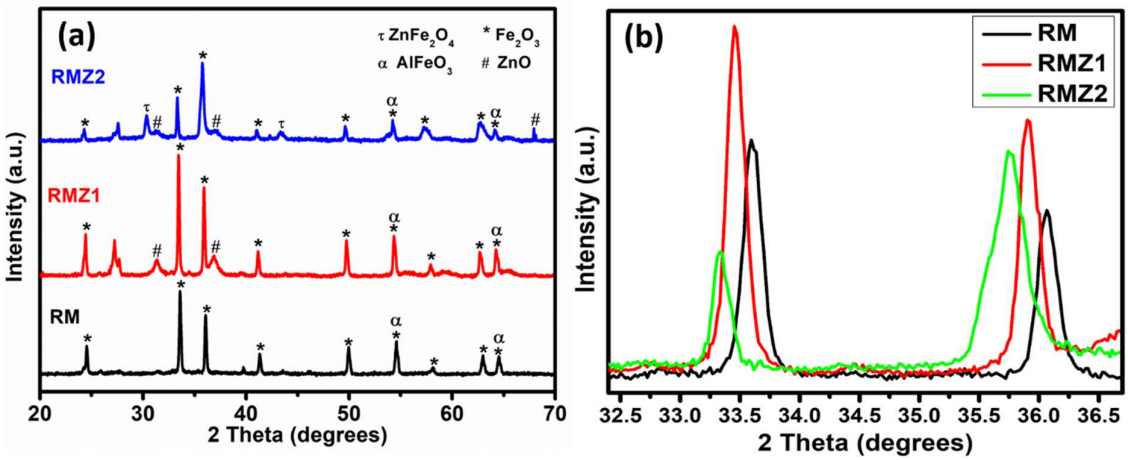

Figure 1. (a) X-ray diffraction pattern of Rm, RMZ1 and RMZ2; (b) Peak shifting in (104) and (110) peaks of RM on doping ZnS.

addition of 10 weight % ZnS in Red mud, two peaks of hexagonal wurtzite ZnO can be observed in the XRD spectra of RMZ1, that has been matched with the JCPDS card number 036-1451 [15]. XRD spectra of RMZ2 shows two additional peaks of zinc ferrite ($ZnFe_2O_4$) along with that of ZnO. The XRD peaks of $ZnFe_2O_4$ has been verified with ICDD card number 00-077-0011 [16].

The distortion created in the Red mud lattice structure on addition of ZnS can be seen in peak shifting and broadening in figure 1(b), that shows the peak shifting towards lower 2 theta values. It indicates tensile strain developed in red mud due to stretching of interplanar spacing by ZnO incorporation. Peak widening in case of RMZ2 indicates smaller crystallite size that has been further verified by SEM images.

Addition of ZnS has created defects by reducing Fe_2O_3 in the form of SO_2 gas during sintering. The crystallite size, dislocation density and microstrain has been evaluated using the Debye-Scherrer equation (eqn 1), Williamson-Smallman equation (eqn 2) and Stokes-Wilson equation (eqn 3) respectively [17,18].

$$D = \frac{K\lambda}{\beta \cos\theta} \text{.....(1)}$$

$$\varepsilon = \frac{\beta}{4 \tan\theta} \text{ ... ...(2)}$$

$$\delta = \frac{1}{D^2} \text{ .....(3)}$$

Here, D is the crystallite size, K is the Scherrer constant having value 0.9, λ is the wavelength of the Cu-Kα radiation (0.15406 nm), β is the full width at half maxima (in radians), θ is the diffraction angle (in radians), ε is the micro strain and δ is the dislocation density. Crystallite size, dislocation density and microstrain of all samples have been listed in table 1. An increase in dislocation density and microstrain in the red mud HEC supports water adsorption and splitting, resulting in enhance current generation.

Table 1: Crystallite size, dislocation density and microstrain of RM, RMZ1 and RMZ2.

Sample	Crystallite size (nm)	Dislocation density (x 10^4)	Microstrain (x 10^4)
RM	41.179	5.93	2.671
RMZ1	40.961	6.76	2.705
RMZ2	33.817	13.03	3.885

Zinc sulfide (ZnS) undergoes oxidation to zinc oxide (ZnO) during the sintering process at temperatures exceeding 500 °C. The resultant ZnO subsequently reacts with ferric oxide (Fe_2O_3), the primary constituent of red mud, to form zinc ferrite ($ZnFe_2O_4$). Literature suggests that the nucleation and growth of zinc ferrite commence at approximately 700 °C and completes at

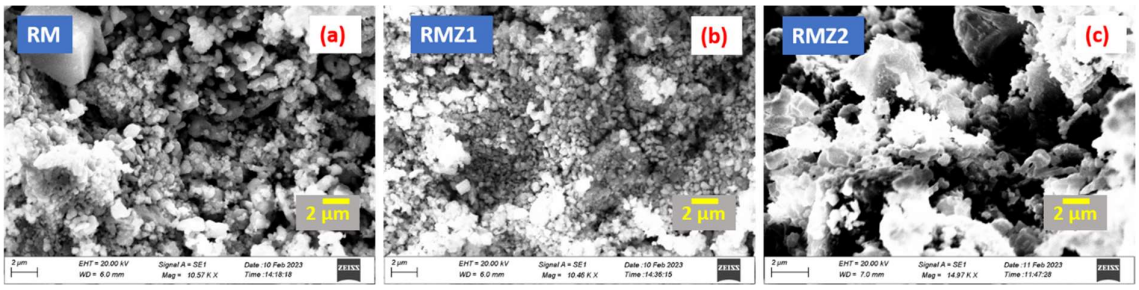

Figure 2. Scanning Electron Microscopy images of (a) RM, (b) RMZ1 and (c) RMZ2.

1300 °C [19]. At a sintering temperature of 800 °C, the initial formation of a disordered zinc ferrite structure is o bserved. The tendency for zinc ferrite formation is directly correlated with zinc oxide concentration [20]. Consequently, no $ZnFe_2O_4$ diffraction peaks were detected in the X-ray diffraction (XRD) pattern of RMZ1, while two distinct $ZnFe_2O_4$ peaks were evident in the XRD pattern of RMZ2 due to an elevated ZnO content arising from higher ZnS content. The disordered zinc ferrite phase along with other oxide components serve as active sites for adsorption and chemidissociation of water by the material, promoting electricity generation in Red mud based Hydroelectric cell.

4.2. Scanning Electron Microscopy (SEM): Scanning electron microscopy has been used to study the particle morphology and pore distribution across the material surface. It can be inferred from the electron micrographs, Figure 2, that all samples consist primarily of nanospheres with a broad particle size distribution. Average particle size has been evaluated using ImageJ software, with RM, RMZ1 and RMZ2 having an average particle size of 0.84, 0.58 and 0.37 µm respectively. Red Mud (figure 2(a)) shows mostly spherical nanoparticles distributed unevenly across the surface. The particle size decreases with increased concentration of ZnS in Red Mud as can be observed in figure 2(b) and (c). Small pores are uniformly distributed throughout the microsphere matrix in RMZ1, whereas RMZ2 shows a highly agglomerated nanoparticle morphology with extensive void spaces. Adding ZnS in RM led to enhanced porosity and surface area facilitating higher surface water adsorption and splitting hence power generation by RMZ1 Hydroelectric cell.

4.3. Mechanism of Green Electricity generation by Hydroelectric Cell: Hydroelectric cell working is based on surface defects like unsaturated surface cations and oxygen vacancies to interact with the water molecules at the material surface. The electrostatic interaction between the surface dangling bonds and dipolar water molecule results in heterolytic splitting of water molecule into H^+ and OH^- ions. This forms a monolayer of chemisorbed OH^- ions on the HEC surface, over which multilayers of water molecules are formed through hydrogen bonding. In the physisorbed layers, H^+ ion interacts with other water molecules and migrate via Grotthus proton hopping mechanism [21]. Since H^+ ion cannot exist alone, it binds with another water molecule to form H_3O^+ i.e. hydronium ion. During chemidissociation and Grotthus proton hopping, some hydronium ions get trapped in the nanopores in the material. These hydronium ions generate an electric field inside the nanopore which leads to physidissociation, thus continuing the water splitting process at the surface. The hydroxide ions (OH^- ions) migrate towards the anode (zinc electrode) where zinc oxidation releases two electrons, simultaneously forming zinc hydroxide [22]. The electrons move via the external circuit towards the cathode (inert silver electrode) where hydronium ions accept electrons and get reduced to hydrogen gas and water [23]. The electrochemical reactions are summarised in equations 4-6.

At surface: $4\ H_2O \rightarrow 2\ H_3O^+ + 2\ OH^-$ ----------(4)

Anode: $Zn + 2\ OH^- \rightarrow Zn(OH)_2 + 2\ e^-$ Eox = 0.76 V ----------(5)

Cathode: $H_3O^+ + 2e^- \rightarrow H_2 + H_2O$ Ered = 0.22 V ----------(6)

The power generated by Red mud and ZnS doped Red mud hydroelectric cells is given in table 2. The cell performance has been further studied by plotting V-I polarization curves of all the samples.

Table 2: Current, voltage and power generated by RM, RMZ1 and RMZ2 HECs.

Composite	Current (mA)	Voltage (V)	Power (mW)
Red Mud (RM)	8.7	0.96	8.35
10 wt % ZnS-Red Mud (RMZ1)	13	0.98	12.74
20 wt % ZnS-Red Mud (RMZ2)	10	0.92	9.2

4.4. V-I Polarization Curves: The voltage drop as a function of increasing load has been studied by plotting V-I polarization curves of all samples. The different voltage loss regions observed in the polarization curves, shown in figure 3, provide insights into the operational characteristics of these HEC device. Experimental results indicate an open circuit voltage (Voc) of 0.96 V for RM, 0.98 V for RMZ1 and 0.92 V for RMZ2, given in table 2. The short circuit current of 8.7 mA observed in RM has been increased to 13 mA and 10 mA in ZnS doped RMZ1 and RMZ2 respectively. Analysis of polarization curves reveals three distinct voltage loss regions. The initial region, at low current densities, primarily reflects activation losses. This voltage drop is attributed to the energy required for water splitting and associated electrochemical processes [24]. The region AB marked in figure 3 represents activation losses due to the sluggish charge transfer at the material-electrode surface. Diminished activation loss region has been observed after doping ZnS in Red mud. Enhanced surface defects

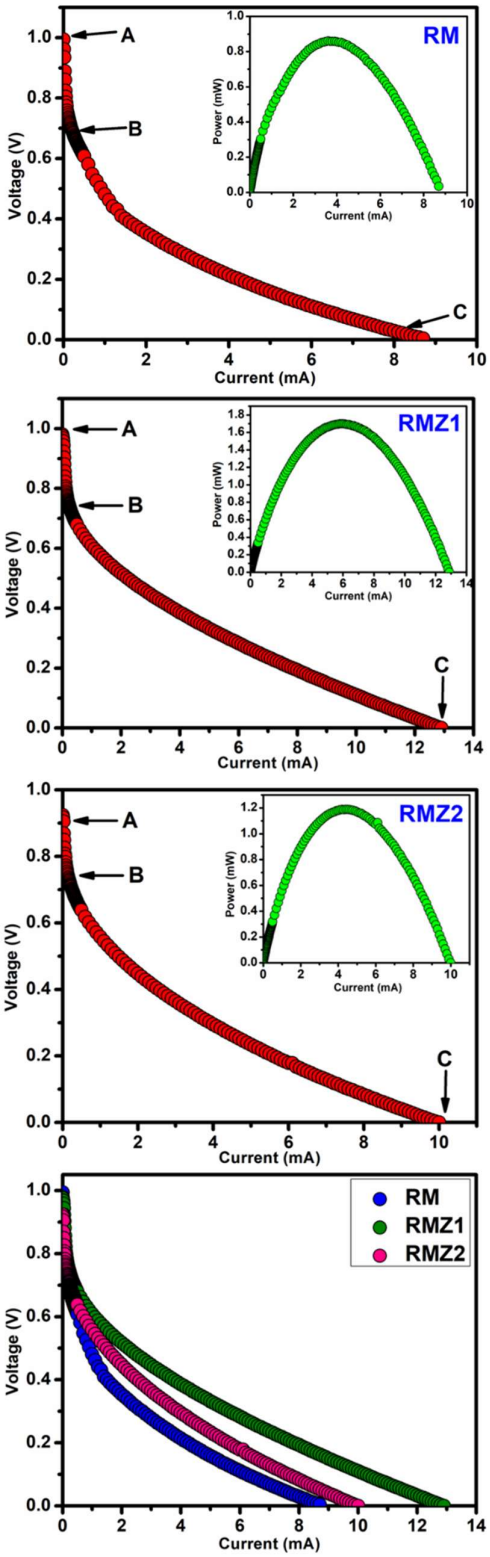

Figure 3. V-I polarization curves of RM, RMZ1 and RMZ2. Last figure presents a comparison of voltage and current relationship in all the samples

and porosity accelerates water chemidissociation at the HEC surface providing large number of ions at the electrode.

The intermediate region BC, exhibits Ohmic losses due to the material's internal resistance faced by the migrating hydronium and hydroxide ions inside the porous structure. At high current densities, concentration losses dominate as ion accumulation on electrode surfaces becomes significant, which is not observed in our case. This might be due to the rapid consumption of ions in the electrochemical reaction at the two active electrodes [12].

The comparative V-I polarization plot of the three samples shows the least voltage losses and hence maximum power generation capacity of RMZ1 Hydroelectric cell.

4.5. Electrochemical Impedance Spectroscopy (EIS): Water splitting as well as the electrochemical reactions occurring in the Hydroelectric cell are limited by the ion movement at and across the material surface. To study the kinetics of charge transfer at electrode-material interface as well as the ionic diffusion inside the bulk material, electrochemical impedance spectroscopy has been carried out.

Nyquist plots of the three wet red mud-ZnS HECs are given in figure 4. Red mud Nyquist plot exhibits a distinct semicircle at high frequency region and a larger incomplete semicircle at lower frequencies. The high-frequency semicircle corresponds to the material's bulk resistance due to grain boundaries and second semicircle is due to impedance faced by the charge transfer reaction at the material-electrode interface [25]. In addition to the semicircle, a slanting tail is also visible in the Nyquist plots of ZnS doped red mud, that represents Warburg impedance region. This low-frequency Warburg impedance is indicative of mass transfer limitations due to hindered ionic diffusion within the material near the electrode surface [26].

In order to determine the individual resistive and capacitive contribution of various species, Nyquist plots have been fitted using EIS Spectrum software. Equivalent circuits models employed in fitting have been depicted in figure 4. The fitting parameters of various circuit elements are given in table 3. Different contributions to impedance spectrum includes, the bulk resistance (R_1), grain boundary resistance (R_2), charge transfer resistance (R_3) and Warburg diffusion (W). The deviation from an ideal capacitive behaviour has been modelled using constant phase elements (P_1, n_1, P_2, n_2) [27].

Doping ZnS into red mud resulted in a decrease in all resistance values, suggesting accelerated ion transport kinetics. The enhanced water adsorption and dissociation capacities of RMZ1 and RMZ2 can be attributed to their smaller particle size, larger surface area, and increased porosity. The lattice defects introduced by ZnS doping facilitates rapid chemisorption and unimpeded charge transfer. The distorted lattice structures of RMZ1 and RMZ2 promotes the diffusion of H_3O^+ and OH^- through the pellet. All these factors collectively contribute in greater power generation capacity of ZnS doped Red mud Hydroelectric cells.

Table 2: Equivalent Circuit fitting parameters for RM, RMZ1 and RMZ2 HECs Nyquist plots.

	RM	RMZ1	RMZ2
R_1	24.53	11.84	16.09
R_2	6.53	2.92	12.00
R_3	80.78	4.48	5.04
W	-	91.68	55.00
P_1	0.03×10^{-4}	5×10^{-4}	39.5×10^{-4}
n_1	0.64	0.54	0.53
P_2	0.00843	0.000475	0.000569
n_2	0.27	0.79	0.43

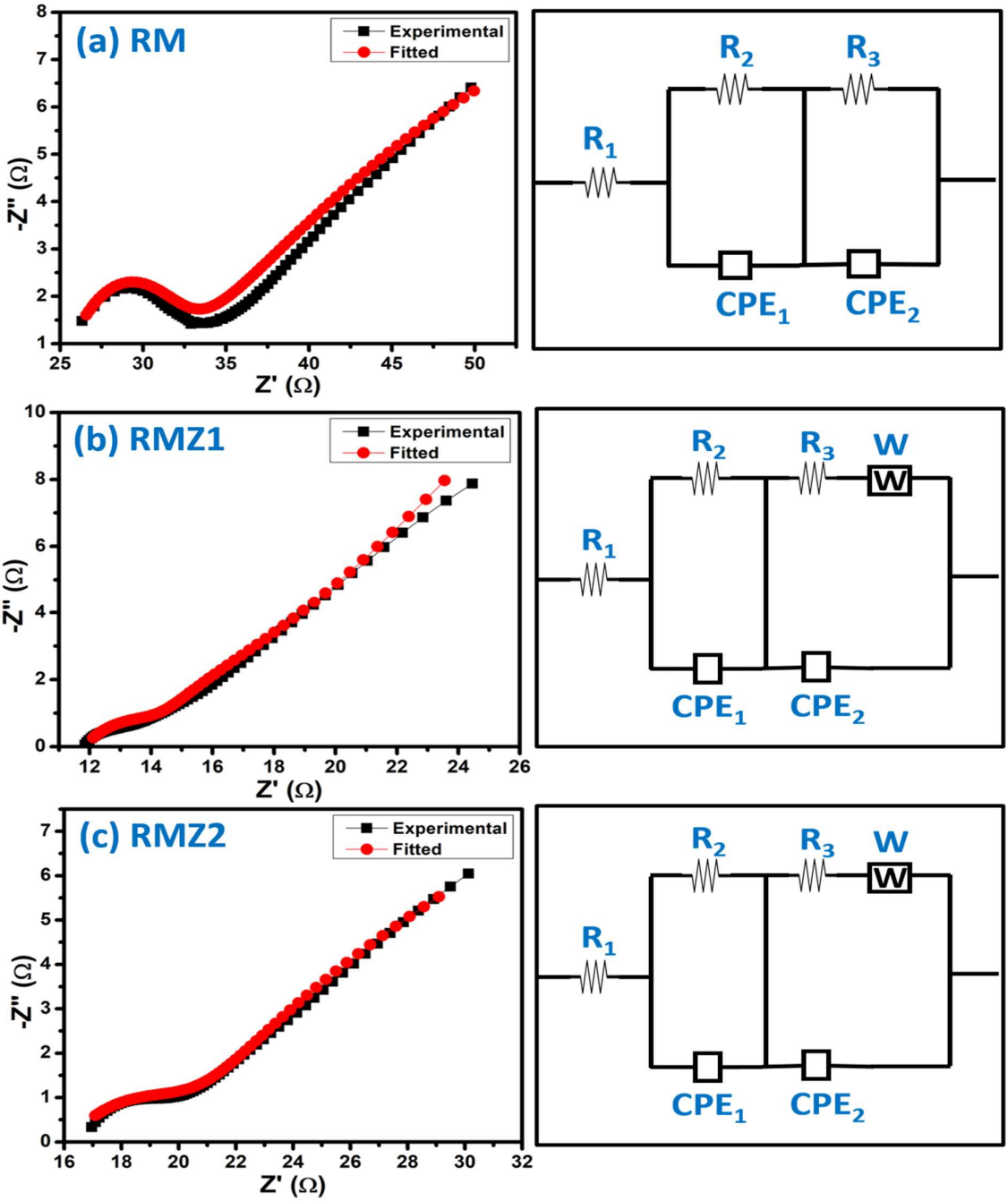

Figure 4. Nyquist plots and corresponding electrical circuit of (a) RM, (b) RMZ1 and (c) RMZ2.

5. Conclusions: In the present study red mud, a toxic industrial waste product, has been transformed into Hydroelectric cell that generates green electricity by water splitting. The red mud Hydroelectric cell's performance has been enhanced by doping zinc sulfide (ZnS) at 10 wt% and 20 wt% concentrations in red mud. XRD analysis revealed significant structural changes in red mud after ZnS doping, including lattice distortions and microstrain arising due to the formation of ZnO and zinc ferrite phases. SEM analysis depicts a reduction in particle size from 0.84 µm in pure red mud (RM) to 0.37 µm in the 20% ZnS-doped sample (RMZ2), along with increased porosity. Activation and Ohmic losses are substantially reduced in RMZ1 and RMZ2

as evidenced by the V-I polarization curves indicating more efficient water splitting and ion transport. The 10 wt% ZnS-doped sample (RMZ1) achieved the highest power output of 12.74 mW, compared to 9.2 mW for RMZ2 and 8.35 mW for pure red mud (RM). EIS spectroscopy results validate the enhanced ionic conductivity and reduced resistance in ZnS doped red mud samples, which is attributed to their smaller particle size, larger surface area, and increased porosity. Hence, the present study shows that the hazardous red mud waste can be effectively translated into a valuable material for clean energy production in the form of Hydroelectric cell. The strategic incorporation of ZnS successfully enhanced the water-splitting capabilities through increased surface defects and porosity. This approach not only addresses the environmental concerns associated with red mud disposal but also presents a sustainable pathway for its utilization in green energy generation.

References:

[1] L. Wang, N. Sun, H. Tang, W. Sun, A review on comprehensive utilization of red mud and prospect analysis, Minerals 9 (2019). https://doi.org/10.3390/min9060362.

[2] M. Archambo, S.K. Kawatra, Red Mud: Fundamentals and New Avenues for Utilization, Mineral Processing and Extractive Metallurgy Review 42 (2021) 427–450. https://doi.org/10.1080/08827508.2020.1781109.

[3] C.R. Borra, B. Blanpain, Y. Pontikes, K. Binnemans, T. Van Gerven, Recovery of Rare Earths and Other Valuable Metals From Bauxite Residue (Red Mud): A Review, Journal of Sustainable Metallurgy 2 (2016) 365–386. https://doi.org/10.1007/s40831-016-0068-2.

[4] L. Wang, G. Hu, F. Lyu, T. Yue, H. Tang, H. Han, Y. Yang, R. Liu, W. Sun, Application of red mud in wastewater treatment, Minerals 9 (2019). https://doi.org/10.3390/min9050281.

[5] W. Huang, S. Wang, Z. Zhu, L. Li, X. Yao, V. Rudolph, F. Haghseresht, Phosphate removal from wastewater using red mud, J Hazard Mater 158 (2008) 35–42. https://doi.org/10.1016/j.jhazmat.2008.01.061.

[6] G. Bhattacharya, S.J. Fishlock, J.S. Roy, A. Pritam, D. Banerjee, S. Deshmukh, S. Ghosh, J.A. McLaughlin, S.S. Roy, Effective Utilization of Waste Red Mud for High Performance Supercapacitor Electrodes, Global Challenges 3 (2019). https://doi.org/10.1002/gch2.201800066.

[7] R.K. Kotnala, R. Das, J. Shah, S. Sharma, C. Sharma, P.B. Sharma, Red mud industrial waste translated into green electricity production by innovating an ingenious process based on Hydroelectric Cell, J Environ Chem Eng 10 (2022). https://doi.org/10.1016/j.jece.2022.107299.

[8] R.K. Kotnala, J. Shah, Green hydroelectrical energy source based on water dissociation by nanoporous ferrite, Int J Energy Res 40 (2016) 1652–1661. https://doi.org/10.1002/er.3545.

[9] R.K. Kotnala, R. Gupta, A. Shukla, S. Jain, A. Gaur, J. Shah, Metal Oxide Based Hydroelectric Cell for Electricity Generation by Water Molecule Dissociation without Electrolyte/Acid, Journal of Physical Chemistry C 122 (2018) 18841–18849. https://doi.org/10.1021/acs.jpcc.8b04999.

[10] S. Jain, J. Shah, S.R. Dhakate, G. Gupta, C. Sharma, R.K. Kotnala, Environment-Friendly Mesoporous Magnetite Nanoparticles-Based Hydroelectric Cell, Journal of Physical Chemistry C 122 (2018) 5908–5916. https://doi.org/10.1021/acs.jpcc.7b12561.

[11] S. Saini, K.L. Yadav, J. Shah, R.K. Kotnala, Enhanced Water Splitting by Strained Lithium-Substituted Nickel Ferrite Hydroelectric Cells, ACS Appl Energy Mater 5 (2022) 8178–8188. https://doi.org/10.1021/acsaem.2c00708.

[12] R. Gupta, J. Shah, R. Singh, R.K. Kotnala, Nonphotocatalytic Water Splitting Process to Generate Green Electricity in Alkali Doped Zinc Oxide Based Hydroelectric Cell, Energy and Fuels 35 (2021) 9714–9726. https://doi.org/10.1021/acs.energyfuels.1c01164.

[13] A. Shukla, S. Badola, J. Shah, Significant Role of Fe3+ Sites on the Activation Energy Barrier at Electrode Interface in SnO2-Fe2O3 Composite Based Hydroelectric Cell, Current Natural Sciences and Engineering 1 (2024) 27–35. https://doi.org/10.63015/2H-2409.1.1.

[14] P. Jain, S. Shankar, O.P. Thakur, Production of Green energy via Water Splitting mechanism by Mn- doped Cobalt Ferrites [Co1-xMnxFe2O4] based Hydroelectric Cells, Current Natural Sciences and Engineering 1 (2024) 137–145. https://doi.org/10.63015/2H-2419.1.2.

[15] S. Badola, J. Shah, A. Gaur, S. Khasa, D.S. Rawal, T.K. Mandal, A.K. Srivastava, R.K. Kotnala, Strategic enhancement of oxygen defects in ZnO from ZnS for water splitting to generate green electricity by hydroelectric cell, Appl Mater Today 34 (2023). https://doi.org/10.1016/j.apmt.2023.101904.

[16] F.S. Volkov, M.A. Kamenskii, E.G. Tolstopjatova, L.A. Voskanyan, N.P. Bobrysheva, O.M. Osmolovskaya, S.N. Eliseeva, Synthesis of ZnFe2O4 Nanospheres with Tunable Morphology for Lithium Storage, Nanomaterials 13 (2023). https://doi.org/10.3390/nano13243126.

[17] A.M. Alsaad, A.A. Ahmad, Q.M. Al-Bataineh, A.A. Bani-Salameh, H.S. Abdullah, I.A. Qattan, Z.M. Albataineh, A.D. Telfah, Optical, Structural, and Crystal Defects Characterizations of Dip Synthesized (Fe-Ni) Co-Doped ZnO Thin Films, Materials 13 (2020) 1737. https://doi.org/10.3390/ma13071737.

[18] M. Hassan, S. Younas, F. Sher, S.S. Husain, S. Riaz, S. Naseem, Room temperature ferromagnetism in single-phase Zn1−x Mn x S diluted magnetic semiconductors fabricated by co-precipitation technique, Applied Physics A 123 (2017) 352. https://doi.org/10.1007/s00339-017-0975-5.

[19] G.A. Kolta, S.Z. El-Tawil, A.A. Ibrahim, N.S. Felix, Kinetics and Mechanism of Zinc Ferrite Formation, Thermochimica Acta, 3, 36 (1980) 359-66. https://doi.org/10.1016/0040-6031(80)87031-6

[20] Iliana Halikia and Evangelia Milona, Kinetic Study of the Solid State Reaction between Alpha-Fe_2O_3 and ZnO for Zinc Ferrite Formation, The Canadian Journal of Metallurgy and Materials Science, 33, (1994) 99-109. https://doi.org/10.1179/cmq.1994.33.2.99

[21] Jyoti Shah, RK Kotnala, Humidity sensing exclusively by physisorption of water vapors on magnesium ferriteSensors and Actuators B: Chemical, 171, (2012) 832-837. https://doi.org/10.1016/j.snb.2012.05.079

[22] Jyoti Shah, Ravinder Kumar Kotnala, Rapid green synthesis of ZnO nanoparticles using a hydroelectric cell without an electrolyte, Journal of Physics and Chemistry of Solids, 108 (2017) 15-20. https://doi.org/10.1016/j.jpcs.2017.04.007

[23] Jyoti Shah, Shipra Jain, Abha Shukla, Rekha Gupta, Ravinder Kumar Kotnala, A

facile non-photocatalytic technique for hydrogen gas production by hydroelectric cell, International journal of hydrogen energy,42, 52, (2017) 30584-30590. https://doi.org/10.1016/j.jpcs.2017.04.007

[24] S. Jain, J. Shah, N.S. Negi, C. Sharma, R.K. Kotnala, Significance of interface barrier at electrode of hematite hydroelectric cell for generating ecopower by water splitting, Int J Energy Res 43 (2019) 4743–4755. https://doi.org/10.1002/er.4613.

[25] P. Vadhva, J. Hu, M.J. Johnson, R. Stocker, M. Braglia, D.J.L. Brett, A.J.E. Rettie, Electrochemical Impedance Spectroscopy for All-Solid-State Batteries: Theory, Methods and Future Outlook, ChemElectroChem 8 (2021) 1930–1947. https://doi.org/10.1002/CELC.202100108.

[26] A.C. Lazanas, M.I. Prodromidis, Electrochemical Impedance Spectroscopy─A Tutorial, ACS Measurement Science Au 3 (2023) 162–193. https://doi.org/10.1021/ACSMEASURESCIAU.2C00070/ASSET/IMAGES/LARGE/TG2C00070_0032.JPEG.

[27] M. Dhall, S. Khasa, A. Hooda, J. Shah, R.K. Kotnala, Nanocomposite NBT-MFO for eco-friendly power generation: Self sustainable hydroelectric cell, Ceram Int 50 (2024) 17570–17592. https://doi.org/10.1016/j.ceramint.2024.02.247.